Recent Developments in Advanced Memory Modeling

A. Makarov, V. Sverdlov, and S. Selberherr

Abstract - We discuss different memory technologies based on new storage information principles, highlight the most promising candidates for future universal memory, and give an overview of modeling methods.

I. Introduction

For many decades charge based memory technologies (DRAM, flash memory, and others) have been successfully scaled down to achieve higher speed and increased density of memory chips at lower bit cost. However, memories based on this storage principle are gradually approaching the physical limits of scalability [1]. This is the reason, why new types of memories based on a different storage principle are gaining momentum.

Apart from good scalability, a new type of memory must also exhibit low operating voltages, low power consumption, high operation speed, long retention time, high endurance, and a simple structure [2].

From new technologies two of the most promising candidates for future universal memory are resistive RAM (RRAM) and spin transfer torque RAM (STTRAM). Currently, RRAM and STTRAM have been demonstrated on 4Mb [3] and 64Mb [4] test chips, respectively. These technologies could be manufacturable on large scale within 5–10 years [5].

II. Resistive Memory Technology

Resistance change memory possesses the simplest structure in the form of a metal–insulator–metal (MIM) sandwich. The electrical conductance of the insulator can be set at different levels by the application of an electric field, and this phenomenon can be used in memory devices. The resistive switching phenomenon is observed in different types of insulators, such as metal oxides, perovskite oxides, chalcogenide materials, and others. Three memory technologies, conductive-bridging RAM (CBRAM), phase-change RAM (PCRAM), and RRAM, are based on the resistive switching.

The concepts of RRAM shown by NDL [6] and Samsung [7] have already surpassed the scaling limit of charge based storage memories [8]. However, a proper fundamental understanding of the RRAM switching mechanism is still missing, hindering further development of this type of memory. First and foremost, one needs a better understanding and control of the physics of the SET/RESET processes through development of accurate models [5].

A.Makarov, V.Sverdlov, and S.Selberherr are with the Institute for Microelectronics, TU Wien, Gußhausstraße 27-29, A-1040 Vienna, Austria, E-mail: Makarov@iue.tuwien.ac.at

In [9], [10] the resistive switching behavior is associated with the formation and rupture of a conductive filament (CF). The CF is formed by localized oxygen vacancies V_o and the conduction is due to electron hopping between these V_o. Rupture of a CF is caused by a redox reaction in the oxide layer under a voltage bias (Fig.1).

In [10], for modeling the resistive switching by Monte Carlo techniques the dynamics of oxygen ions (O^{2-}) and electrons in an oxide layer was described as follows:

- formation of V_o by O^{2-} moving to an interstitial position;
- annihilation of V_o by moving O^{2-} to V_o;
- an electron hop into V_o from an electrode;
- an electron hop from V_o to an electrode;
- an electron hop between two V_o.

In order to describe the dependences of transport on the applied voltage and temperature the hopping rates for electrons are chosen as [11]:

$$\Gamma_{nm} = A_e \cdot \frac{\Delta E_{nm}}{\hbar \cdot \left(1 - \exp\left(-\Delta E_{nm} / k_B T\right)\right)} \cdot \exp\left(-R_{nm} / a\right) \quad (1)$$

Here, $\hbar$ is the Planck constant, A_e is a dimensionless coefficient, ΔE_{nm} is the difference between the energies E_n and E_m of an electron positioned at the site n and m, respectively, R_{nm} is the hopping distance, a is the localization radius, T is the temperature, and k_B is the Boltzmann constant. When an external voltage U is applied, the energy difference ΔE_{nm} includes the corresponding voltage dependent term:

$$\Delta E_{nm} = E_n - E_m + \frac{U}{d} \cdot \Delta x \quad (2)$$

Here, d is the x-dimension of the system, $\Delta x = x_m - x_n$ is the difference between the x coordinate of the sites (vacancies) m and n.

The rates (1) are similar to those used in single-electron transport theory. The exponential in the denominator guarantees an exponentially small equilibrium occupation of a site m as compared to the occupation of a site n, if the condition $E_m - E_n >> k_B T$ is satisfied. When the opposite condition $E_n - E_m >> k_B T$ is fulfilled, the rate is proportional to the external field U/d. Therefore, the rates (1) can mimic an Ohmic (linear in external field) transport in a system of equivalent sites having the same energy, if the temperature T is small.

978-1-4673-0235-7/12/$31.00 © 2012 IEEE

The hopping rates between an electrode (0 or 2N) and an oxygen vacancy m are described by:

$$\Gamma_{0m}^{iC} = \alpha \cdot \Gamma_{0m}, \Gamma_{m0}^{oC} = \alpha \cdot \Gamma_{m0} \quad (3)$$

$$\Gamma_{(2N)m}^{iA} = \beta \cdot \Gamma_{(2N)m}, \Gamma_{m(2N)}^{oA} = \beta \cdot \Gamma_{m(2N)} \quad (4)$$

Here, α and β are the coefficients of the boundary conditions on the cathode and anode, respectively, N is the number of sites, A and C stand for cathode and anode, respectively, and i and o for hopping on the site and out from the site. Contrary to an oxygen vacancy, an electrode is assumed to have enough electrons so that hopping from an electrode to a vacancy is always allowed, provided the vacancy was empty before the event. Complimentary, an electrode has always a place to accept a carrier, so an electron can always hop at an electrode, provided this event is allowed.

The current generated by hopping is calculated as:

$$I = q_e \cdot \frac{\sum \Delta x}{d \cdot \sum t} \quad (5)$$

Here, q_e is the electron charge,

$t = \left(\sum_{m,n=0}^{2N} \Gamma_{mn} f_m (1 - f_n) \right)^{-1}$ is the time spent for moving an electron at a distance Δx, f_n=1 (0), if the site n is occupied (empty), $f_0 = \alpha$ and $f_{2N} = \beta$, if an electron hops from an electrode, and $(1- f_0) = \alpha$ and $(1- f_{2N}) = \beta$, if a hop to an electrode occurs. Thus, $q_e \Delta x/d$ is a charge passing through an external circuit during a single hopping event. The summation in (5) is over all hopping events. Therefore, (5) gives the current as the total charge passing through the external circuit during the total time $\sum t$.

To describe the field-induced ion dynamics the ion rates are chosen similar to (1):

$$\Gamma_n^{'} = A_i \cdot \frac{\Delta E}{\hbar \cdot (1 - \exp(-\Delta E / k_B T))} \quad (6)$$

Here we assume that O^{2-} can move from the lattice site to the nearest interstitial, provided the interstitial is empty. Alternatively, O^{2-} can move back from the interstitial to the nearest vacancy, provided it is not occupied by an electron. A distance-dependent term is thus included in the dimensionless coefficient A_i. When an external voltage is applied, the difference in energy of an ion before and after hopping is computed as

$$\Delta E = \frac{U}{d} \cdot x - E_c \quad (7)$$

E_c is a threshold energy for the m-th vacancy V_o formation /annihilation energy of the m-th vacancy V_o, when O^{2-} is moving to an interstitial or back to V_o, respectively. The values of these energies depend on the insulating material.

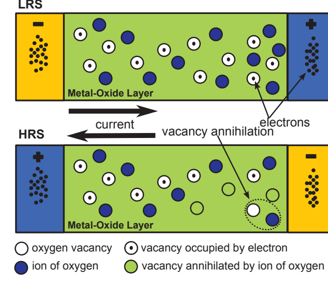

Figure 1. Schematic illustration of the conducting filament in the low resistance state (LRS) and hight resistance state (HRS).

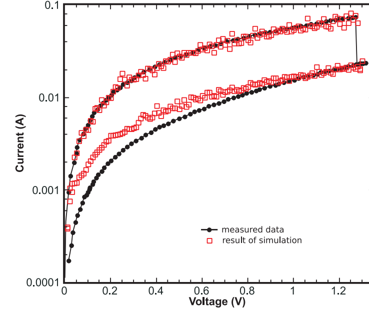

Figure 2. Current-voltage curves during the reset process. The lines are measured results from [9]. The symbols are obtained from the model [10].

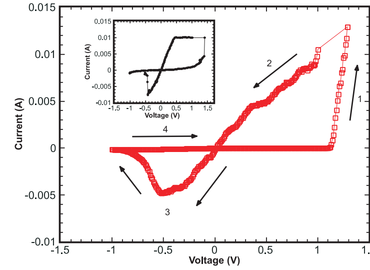

Figure 3. I-V characteristics showing the hysteresis cycle obtained from the model [10]. The inset shows the hysteresis cycle for M-ZnO-M from [12].

Results of simulations obtained with the model [10] are shown in Fig.2 and Fig.3. Fig.2 shows the RESET process for a single CF, which is in good agreement with the measurements from [9].

Fig.3 shows the RRAM switching hysteresis cycle. The simulated cycle is in agreement with the experimental cycle from [12] shown in the inset of Fig.3. The interpretation of the RRAM hysteresis cycle obtained from the stochastic model is as follows. If a positive voltage is applied, the formation of a CF begins, when the voltage reaches a critical value sufficient to create V_o by moving O^{2-} to an interstitial position. The formation of the CF leads to a sharp increase in the current (Fig.3, Segment 1) signifying a transition to a state with low resistance. When a reverse negative voltage is then applied, the current increases linearly, until the applied voltage reaches the value at which an annihilation of V_o is triggered by means of moving O^{2-} to V_o. The CF is ruptured and the current

decreases (Fig.3, Segment 3). This is the transition to a state with high resistance.

III. Magnetic Memory Technology

The basic element of an MRAM is a magnetic tunnel junction (MTJ), a sandwich of two magnetic layers separated by a thin non-magnetic spacer. While the magnetization of the pinned layer is fixed due to the fabrication process, the magnetization direction of the free layer can be switched between the two states parallel and anti-parallel to the fixed magnetization direction. Switching in MRAM is performed by applying a magnetic field. In contrast to field-driven MRAM, STTRAM does not require an external magnetic field. Switching between the two states occurs due to the spin-polarized current flowing through the MTJ.

The micromagnetic simulations are based on the magnetization dynamics described by the Landau-Lifshitz-Gilbert equation:

$$\frac{dm}{dt} = -\frac{\gamma}{1+\alpha^2}\cdot\left(\left(m\times h_{eff}\right)+\alpha\cdot\left[m\times\left(m\times h_{eff}\right)\right]+ \right.$$
$$+\frac{g\mu_B j}{e\gamma M_s d}\cdot\left(g_1(\theta_1)\cdot\left(\alpha\cdot(m\times p_1)-\left[m\times(m\times p_1)\right]\right)-\right. \quad (8)$$
$$\left.\left.-g_2(\theta_2)\cdot\left(\alpha\cdot(m\times p_2)-\left[m\times(m\times p_2)\right]\right)\right)\right).$$

Here, γ is the gyromagnetic ratio, α is the Gilbert damping parameter, g is the gyromagnetic splitting factor, μ_B is Bohr's magneton, j is the current density, e is the electron charge, d is the thickness of the free layer, $m=M/M_s$ is the position dependent normalized vector of the magnetization in the free layer, $p_1=M_{p1}/M_{sp1}$ and $p_2=M_{p2}/M_{sp2}$ are the normalized magnetization of the first and second pinned layers, respectively. M_s, M_{sp1}, and M_{sp2} are the saturation magnetization of the free layer, the first pinned layer, and the second pinned layer.

Slonczewski's expressions are used for the MTJ with a dielectric layer [13]

$$g_1(\theta) = 0.5\cdot\eta\cdot\left[1+\eta^2\cdot\cos(\theta)\right]^{-1} \quad (9)$$

and with a metal layer [14]

$$g_2(\theta) = \left[-4+(1+\eta)^3(3+\cos(\theta))/4\eta^{3/2}\right]^{-1} \quad (10)$$

between the ferromagnetic contacts, respectively. In the penta-layer structure (Fig.4) the two spin torques are acting independently on the two opposite interfaces of the free ferromagnetic layer, provided its thickness is larger than the scale on which the electron spins entering into the ferromagnet become aligned to the ferromagnet's magnetization.

The local effective field is calculated as:

$$h_{eff} = h_{ext} + h_{ani} + h_{exch} + h_{demag} + h_{th} + h_{amp} + h_{ms}. \quad (11)$$

Here, h_{ext} is external field, h_{ani} is anisotropic field, h_{exch} is an exchange field, h_{demag} is a demagnetizing field, h_{th} is a thermal field, h_{amp} is the Ampere field, and h_{ms} is the

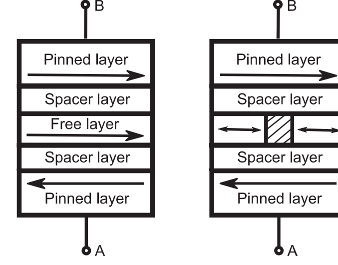

Figure 4. Schematic illustration of the penta-layer MTJ with monolithic (left) and composite free layer (right).

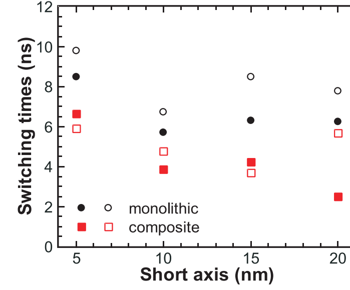

Figure 5. The absolute values of the switching times for MTJs with monolithic and composite free layer as function of the short axis. The long axis is fixed at 52.5nm. The thickness of the free layer is 3.5nm (filled symbols) and 4nm (open symbols).

magnetostatic coupling between the pinned layers and the free layer.

In case of uniaxial anisotropy the anisotropic field is [15]:

$$h_{ani} = \frac{2K_1}{\mu_0 M_s}(m\cdot u)u, \quad (12)$$

while for cubic anisotropy it is calculated as:

$$h_{ani} = -\frac{2D}{\mu_0 M_s}m. \quad (13)$$

Here, D is the diagonal matrix with entries

$$D_{11} = K_1(m_y^2+m_z^2)+K_2 m_y^2 m_z^2, \quad (14)$$
$$D_{22} = K_1(m_x^2+m_z^2)+K_2 m_x^2 m_z^2, \quad (15)$$
$$D_{33} = K_1(m_x^2+m_y^2)+K_2 m_x^2 m_y^2, \quad (16)$$

K_1 and K_2 are the material-dependent anisotropy coefficients, u is the easy axis, μ_0 is the magnetic constant.

The exchange field is calculated as [15]:

$$h_{exch} = \frac{2A}{\mu_0 M_s}\sum_j((m_j-m)/|r_j|^2). \quad (17)$$

Here, A is the exchange constant.

For calculating the demagnetization field the method proposed in [16] is used.

The thermal field is calculated as [17]:

$$h_{th} = \sigma\cdot\sqrt{\frac{\alpha}{1+\alpha^2}\cdot\frac{2k_B T}{\gamma\Delta V\Delta t M_s}}. \quad (18)$$

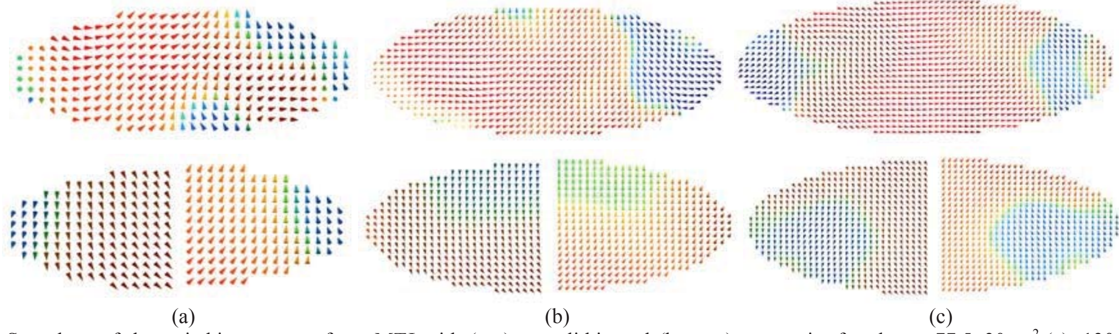
(a) (b) (c)

Figure 6. Snapshots of the switching process for a MTJ with (top) monolithic and (bottom) composite free layer: 77.5×30nm^2 (a), 130×50nm^2 (b), 155×60nm^2 (c). The direction of the magnetization is shown as the unit vectors, color indicates the *x*-component of the magnetization, the *x*-axis is directed along the long axis of the ellipse.

Here, σ is a Gaussian random uncorrelated function, k_B is the Boltzmann constant, ΔV is the volume of cell, Δt is the time step.

The eddy currents' field is [18]:

$$h_{amp} = \sum_{j=1...N} \frac{J_j}{4\pi} \times \int_j \frac{r_i - r_j}{r^3} dv. \qquad (19)$$

Here, J_j is the current induced on a cell (j:1. . .N).

Measurements [19] showed a decrease in the critical current density for the penta-layer structure. An even more pronounced decrease of the switching current density was recently reported in a penta-layer structure with a composite free layer (Fig.4, right) [20]. In addition, as shown in Fig.5, also the switching time decreases in the penta-layer structure with the composite free layer for the same current density. When the central region is removed, the end domains become virtually independent and switch without forming domain walls (Fig.6).

IV. Conclusion

Two of the most promising candidates for future universal memory are the RRAM and STTRAM. Material and structure optimization through accurate modeling and simulation is key in successfully designing future memory cells with low power consumption.

Acknowledgement

This research is supported by the European Research Council through the grant #247056 MOSILSPIN.

References

[1] S. Hong, "Memory technology trend and future challenges," *IEEE Intl. Electron Dev. Meet.*, p.292, 2010.

[2] M.H. Kryder, C.S. Kim, "After hard drives – what comes next?" *IEEE Trans. Magn.*, vol. 45, p.3406, 2009.

[3] S-S Sheu, M-F Chang, K-F Lin, et al., "A 4Mb embedded SLC resistive-RAM macro with 7.2ns read–write random-access time and 160ns MLC-access capability," *IEEE ISSCC*, p.200, 2011.

[4] K. Tsuchida, T. Inaba, K. Fujita, et al., "A 64Mb MRAM with clamped-reference and adequate-reference schemes," *IEEE ISSCC*, p.258, 2010.

[5] ITRS Roadmap can be downloaded from the following URL: http://www.itrs.net/

[6] C.H. Ho, C-L Hsu, C-C Chen, et al., "9nm half-pitch functional resistive memory cell with <1μA programming current using thermally oxidized sub-stoichiometric WOx film," *IEEE Intl. Electron Dev. Meet.*, p.436, 2010.

[7] M.J. Kim, I.G. Baek, Y.H. Ha, et al., "Low power operating bipolar TMO ReRAM for sub 10nm era," *IEEE Intl. Electron Dev. Meet.*, p.444, 2010.

[8] W.C. Chien, F.M. Lee, Y.Y, Lin, et al., "Current status and future challenges of resistive switching memories," *SSDM*, p.1003, 2011.

[9] B. Gao, B. Sun, H. Zhang, et al., "Unified physical model of bipolar oxide-based resistive switching memory," *IEEE Electron Dev. Lett.*, vol. 30, p.1326, 2009.

[10] A. Makarov, V. Sverdlov, S. Selberherr, "Stochastic model of the resistive switching mechanism in bipolar resistive random access memory: Monte Carlo simulations," *J. Vac. Sci. Technol. B*, vol. 29, p.01AD03, 2011.

[11] V. Sverdlov, A.N. Korotkov, K.K. Likharev, "Shot-noise suppression at two-dimensional hopping," *Phys. Rev. B*, vol.63, p.081302, 2001.

[12] S. Lee, H. Kim, D.J. Yun, et al., "Resistive switching characteristics of ZnO thin film grown on stainless steel for flexible nonvolatile memory devices," *Appl. Phys. Lett.*, vol.95, p.262113, 2009.

[13] J. Slonczewski, "Currents, Torques, and polarization factors in magnetic tunnel junctions," *Phys. Rev. B*, vol.71, p.024411, 2005.

[14] J. Slonczewski, "Current-driven excitation of magnetic multilayers," *J. Magn. Magn. Mater.*, vol.159, p.L1, 1996.

[15] J.E. Miltat, M.J. Donahue, "Numerical Micromagnetics: Finite Difference Methods," Handbook of Magnetism and Advanced Magnetic Materials. John Wiley & Sons, Ltd., 2007.

[16] A. Kákay, "Numerical Investigations of Micromagnetic Structures," Ph.D. Thesis. Research Institute for Solid State Physics and Optics, Budapest, 2005.

[17] K. Ito, T. Devolder, C. Chappert, et al., "Probabilistic behavior in subnanosecond spin transfer torque switching," *J. Appl. Phys.*, vol.99, p.08G519, 2006.

[18] L. Torres, L. Lopez-Diaz, E. Martinez, et al. "Micromagnetic dynamic computations including eddy currents." *IEEE Trans. Magn.*, vol.39, p.2498, 2003.

[19] G.D. Fuchs, I.N. Krivorotov, P.M. Braganca, et al., "Adjustable spin torque in magnetic tunnel junctions with two fixed layers," *Appl. Phys. Lett.*, vol. 86, p.152509, 2005.

[20] A. Makarov, V. Sverdlov, S. Selberherr, "Reduction of switching time in pentalayer magnetic tunnel junctions with a composite-free layer," *Phys.Status Solidi RRL*, vol.5, p.420, 2011.